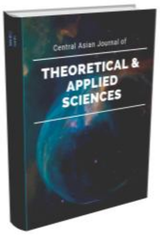

CENTRAL ASIAN JOURNAL OF THEORETICAL AND APPLIED SCIENCE

https://cajotas.centralasianstudies.org/index.php/CAJOTAS

Volume: 06 Issue: 04 | October 2025 ISSN: 2660-5317

Article

Theoretical Study of Amide Derivative as Corrosion Inhibitor

Maha M. Mahmood[1]*, Khalida A. Samawi[2], Jawad K. Sheine[3]

1. Department of Chemistry, College of Science, AL-Nahrain University, Iraq
2. Department of Chemistry, College of Science, AL-Nahrain University, Iraq
3. Department of Chemistry, College of Science, AL-Nahrain University, Iraq

*Correspondence: mmaahhaaa1998@gmail.com

Abstract: Quantum simulations using semi-empirical PM3 and Density Functional Theory (DFT) techniques based on B3LYP/(6-311G), (2d,2p) were used to theoretically investigate corrosion inhibitors. Essential quantum chemistry parameters, such as E_{HOMO} (highest occupied molecular orbital energy) and E_{LUMO} (lowest molecular orbital energy), were found to correlate with the effectiveness of amide derivative N-((1R)-((3a,7a-dihydrobenzo [d] thiazol-2-yl)thio) (pyridin-2-yl)methyl)-N-(4-nitrophenyl) acetamide compound [A] as corrosion inhibitor. Energy gap, electron affinity (EA), hardness (EA), dipole moment (μ), softness (S), ionization potential (IE), absolute electron negativity (χ), and global electrophilicity index (ω) are among the other parameters that are also examined. By pointing out reactive centers and possible locations for nucleophilic and electrophilic assaults, the Mulliken population was also crucial in determining a local reactivity. Theoretical predictions indicate that the compound [A] is superior as a corrosion inhibitor.

Keywords: corrosion inhibitor, Amide, Hardness, Softness.

Citation: Mahmood, M. M., Samawi, K. A & Sheine, J. K. Theoretical Study of Amide Derivative as Corrosion Inhibitor. Central Asian Journal of Theoretical and Applied Science 2025, 6(4), 653-661

Received: 10th May 2025
Revised: 16th Jun 2025
Accepted: 24th Jul 2025
Published: 12th Aug 2025

1. Introduction

A corrosion inhibitor is a chemical compound that interacts with a metal surface or surrounding environment to prevent corrosion on the metal's surface [1]. Corrosion inhibitors are usually organic molecules with heterogeneous atoms (sulfur, oxygen, and nitrogen) in their aromatic composition [2]. Organic compounds frequently have a propensity to withstand corrosion due to the high electron density on heterogeneous atoms [3]. These organic compounds' inhibitory effect is typically ascribed to their adsorption interactions with the metal surface. The reaction center that stabilizes the adsorption process is thought to be polar functional groups [4]. To solve the chemical conundrum and explain the mechanism of the corrosion reaction, quantitative chemical calculations were employed [5-8]. This method works well for examining the inhibitor molecule's mechanism of action on the metal surface. The use of chemical inhibitors is one such technique. High electron-level elements like N, O, and S are found in the structures of amides, which are organic compounds. Numerous study studies have examined the connection between these amides chemical structures and their inhibitory efficiency [9]. Quantum chemical computations have demonstrated significant efficacy in investigating corrosion inhibition mechanisms. A highly helpful framework for creating new standards for logically analyzing, forecasting, and ultimately comprehending a variety of chemical processes has been made available by density functional theory (DFT). DFT naturally incorporates a number of chemical notions that are now commonly employed as descriptors of chemical reactivity, such as electronegativity, hardness or softness values, etc. [10].

2. Methods and Materials

By examining their quantum mechanical calculations for corrosion inhibition efficiency as a superior corrosion inhibitor over the other using PM3 and DFT methods, the newly prepared derivative of compound [A], as shown in (Fig. 1), will be the subject of this investigation of corrosion inhibition efficiency parameters.

3. Results and Discussion

Optimize geometry of compound [A]

The molecules corresponding geometries were fully optimized using the PM3 semi-empirical method and Density Functional Theory (DFT), which was conducted using Becke's three-parameter functional and the correlation functional of Lee, Yang, and Parr (B3LYP) with a 6-311++G (2d, 2p) level of theory. The molecules were constructed using the Gauss View 09 implemented in the Gaussian 09 package [3]. The geometry of compound [A] is given in Figure 1.

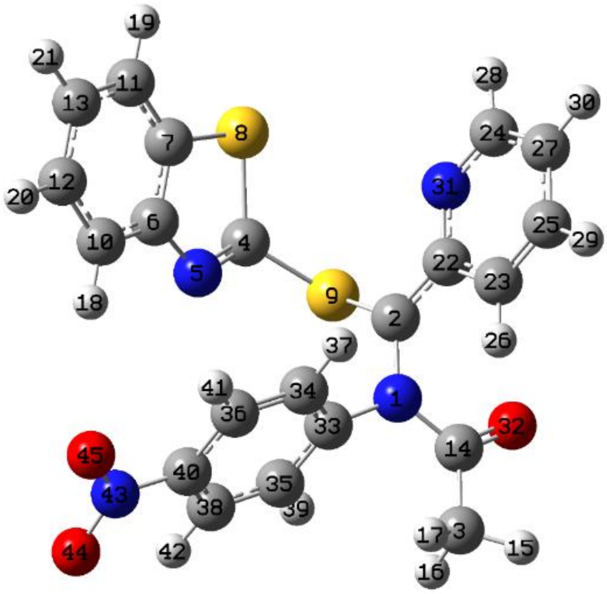

Figure 1. The optimized molecular structure of compound [A] along with the numbering of atoms.

The compound [A] chemical bonds are displayed in Table (1). The carbon–carbon bonds in benzene are not of equal length, which is explained by the existence of a fused thiazole ring. The bond lengths for this chemical range from 1.07865 Å to 1.87675 Å. Nonetheless, there aren't many variations among the six C-C distances. Because of the thiazole moiety's fusion at these carbon atoms, the C_6–C_7 bond has the largest bond distance. The C_4-S_8 bond length is equal to 1.87675, Because the pure single bond feature the C_4-S_8 is longest bond [11].

Table 1. The bond length of compound [A] calculated by using PM3 and DFT (6-311G/ B3LYP).

Description of bond length	**Bond lengths (Å)**	
	PM3	**DFT (6-311G/ B3LYP)**
N_1-C_2	1.42766	1.42707
C_2-S_9	1.78631	1.85795
C_2-C_{22}	1.45063	1.41359
C_4-S_8 (Benzothiazole)	1.75935	1.87675
C_4-S_9 (Benzothiazole)	1.72248	1.83585

C_4-N_5 (Benzothiazole)	1.24333	1.26510
C_6-C_7 (Benzothiazole)	1.41994	1.41070
C_7-C_{11} (Benzothiazole)	1.39234	1.38726
C_6-C_{10} (Benzothiazole)	1.40452	1.40339
C_{10}-C_{12} (Benzothiazole)	1.38954	1.39800
C_{14}-N_1	1.43140	1.40032
C_{14}-C_3	1.50727	1.51829
C_{14}-O_{32}	1.22537	1.24485
C_{33}-N_1	1.45819	1.43085
C_{33}-C_{34} (Benzene)	1.42144	1.41142
C_{34}-C_{36} (Benzene)	1.36800	1.38508
C_{36}-H_{41} (Benzene)	1.09615	1.07865
C_{40}-N_{43}	1.42479	1.42460
N_{43}-O_{44}	1.23435	1.29539
C_{22}-C_{23} (Pyridine)	1.41348	1.43270
C_{22}-N_{31} (Pyridine)	1.37371	1.38121
C_{23}-C_{25} (Pyridine)	1.39184	1.38397
C_{24}-C_{27} (Pyridine)	1.40226	1.39807
C_{24}-N_{31} (Pyridine)	1.34655	1.34054
C_{35}-H_{39} (Arom.+Aliph.)	1.09524	1.08041

Bond angle data for the compound [A] are displayed in Table (2). Because nitrogen has a higher electronegativity than sulfur, the bond angle <C7S8C4 is much less (89.873°) than the bond angle <C4N5C6 (118.731°) [11]. While the <$N_5C_6C_{10}$ and <$C_{11}C_7S_8$ are larger value due to electronic delocalization effect [12].

Table 2. The bond angle of compound [A] calculated by using PM3 and DFT (6-311G/ B3LYP).

Description of bond angles	**Bond angle(deg)**		**Description of bond angles**	**Bond angle(deg)**	
	PM3	**DFT (6-311G/ B3LYP)**		**PM3**	**DFT (6-311G/ B3LYP)**
$N_1C_{14}C_3$	117.805	117.601	$C_{22}C_{23}H_{26}$	119.864	119.516
$N_1C_{14}O_{32}$	119.424	121.786	$C_{22}C_{23}C_{25}$	119.609	120.018
$C_3C_{14}O_{32}$	122.662	120.573	$C_{23}C_{25}H_{29}$	120.087	119.744
$C_{14}C_3H_{15}$	111.669	107.328	$C_{23}C_{25}C_{27}$	110.535	119.951
$C_{14}C_3H_{16}$	110.911	110.536	$C_{25}C_{27}H_{30}$	120.935	121.778
$C_{14}C_3H_{17}$	110.592	113.284	$C_{25}C_{27}C_{24}$	118.774	117.234
$N_1C_2S_9$	117.995	115.506	$C_{27}C_{24}H_{28}$	122.294	120.541
$C_2S_9C_4$	103.980	108.705	$C_{27}C_{24}N_{31}$	122.132	124.375
$S_9C_4N_5$	124.437	120.677	$C_{24}N_{31}C_{22}$	119.896	119.101
$C_4N_5C_6$	112.706	118.731	$C_2N_1C_{33}$	116.273	114.782
$N_5C_6C_7$	113.056	113.242	$C_{14}N_1C_{33}$	117.660	123.142
$C_6C_7C_{11}$	121.074	119.644	$N_1C_{33}C_{35}$	119.970	120.843
$C_6C_7S_8$	111.142	110.953	$N_1C_{33}C_{34}$	120.465	120.142
$C_7S_8C_4$	91.132	89.873	$C_{33}C_{34}H_{37}$	119.571	118.883

$C_7C_6C_{10}$	121.090	119.930	$C_{33}C_{34}C_{36}$	120.155	120.800
$S_8C_4N_5$	111.789	106.823	$C_{34}C_{36}H_{41}$	119.760	121.619
$S_8C_4S_9$	123.755	122.914	$C_{34}C_{36}C_{40}$	121.012	119.659
$N_5C_6C_{10}$	125.789	126.829	$C_{36}C_{40}N_{43}$	120.963	120.040
$C_6C_{10}H_{18}$	120.744	120.828	$C_{22}C_{23}H_{26}$	119.864	119.516
$C_6C_{10}C_{12}$	118.015	118.715	$C_{22}C_{23}C_{25}$	119.609	120.018
$C_{10}C_{12}H_{20}$	119.377	118.928	$C_{23}C_{25}H_{29}$	120.087	119.744
$C_{10}C_{12}C_{13}$	121.091	121.144	$C_{23}C_{25}C_{27}$	110.535	119.951
$C_{12}C_{13}C_{11}$	120.979	120.111	$C_{36}C_{40}N_{43}$	120.963	120.040
$C_{11}C_7S_8$	129.210	127.956	$C_{40}N_{43}O_{44}$	121.597	119.085
$S_9C_2C_{22}$	121.628	122.416	$C_{40}N_{43}O_{45}$	121.243	118.577
$C_2C_{22}N_{31}$	118.794	118.682	$C_{36}C_{40}C_{38}$	117.991	120.228
$C_2C_{22}C_{23}$	121.115	121.991	$C_{40}C_{38}H_{42}$	119.325	118.628
$C_{22}C_{23}H_{26}$	119.864	119.516	$C_{40}C_{38}C_{35}$	120.934	119.664
$C_{22}C_{23}C_{25}$	119.609	120.018	$C_{38}C_{35}H_{39}$	120.429	120.031
$C_{23}C_{25}H_{29}$	120.087	119.744	$C_{38}C_{35}C_{33}$	120.324	120.788
$C_{23}C_{25}C_{27}$	110.535	119.951	$C_{33}C_{35}H_{39}$	119.294	119.157

Molecular Orbital

The band gap energy value is an important measure for determining molecule electrical transport capabilities. Table (5) shows the energetic properties of compound [A], energy value of HOMO and LUMO orbitals are equal to -1.1486 eV and -0.3246 eV respectively. The E_{gap} of compound [A] is equal to 0.8239 eV for DFT that indicates lesser electrical stability and increased chemical reactivity compared to PM3 that is equal to 5.3491 eV [13].

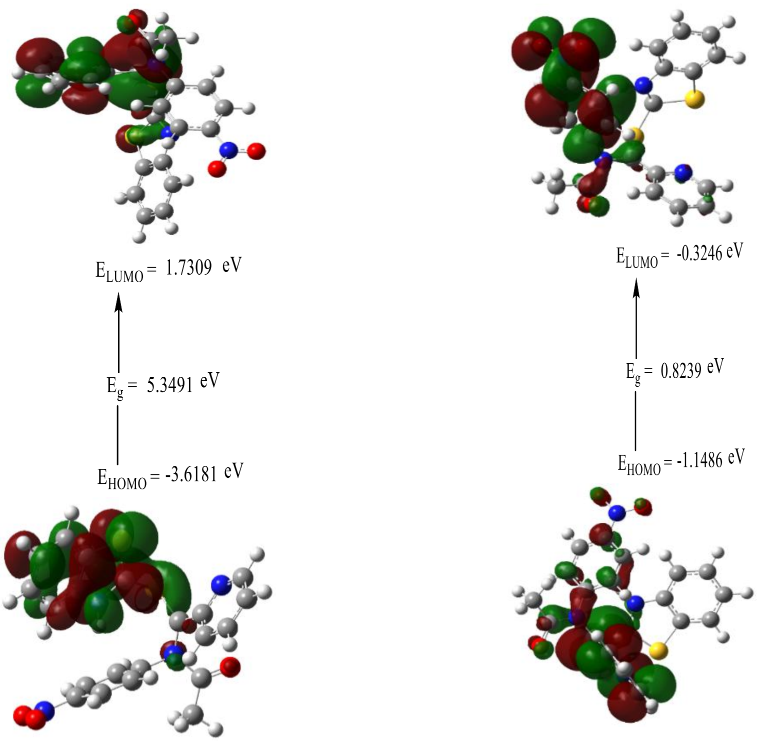

Figure 2. The HOMO and LUMO for compound [A] using the PM3 and DFT.

Global Molecular Reactivity

Adsorption inhibitor compounds and their interactions with metals can be predicted with great help from limits orbital theory. The energy gap between E_{HOMO} and E_{LUMO} ($\Delta E = E_{LUMO}-E_{HOMO}$) indicates that the frontier molecular orbital (FMO) can readily produce theoretical conclusions. The high morale of E_{HOMO} is the propensity to donate electrons to the acceptor with a low-energy molecular orbital vacant, while the energy HOMO (E_{HOMO}) is the capacity to donate an electron to an acceptor. The LUMO (E_{LUMO}) energy parameter describes the molecule capacity to take an electron. For a larger electron-compliant capacity, this is the lowest value. According to the description of the molecular activity, the inhibitor's efficiency increased when the energy gap shrank [14]. The following is the relationship between the HOMO and LUMO energies and the ionization energy (IE) and electronic affinity (EA) [15]:

Ionization potential (IE) = $-E_{HOMO}$ ……………….. (1)

Ionization potential, or IE, is equal to the $-E_{HOMO}$ energy required to extract an electron from an atom. Great inhibitory efficiency is provided by the low ionization energy [14].

Electron affinity (EA) = $-E_{LUMO}$ ……………….. (2)

When one electron is added to a neutral atom, the electron affinity (EA) is equal to the $-E_{HOMO}$ amount of free energy (EA). A low hardness value results in less stability and higher inhibitory efficiency. It has been determined that the second unoriginal of the E is hardness (η). It gauges both molecule reactivity and stability [16]. The HOMO and LUMO of energy are connected to this pace.

Hardness (η) = (IE - EA) / 2 ……………….. (3)

A low electronegativity number indicates a higher inhibitory efficiency.

Electronegativity (χ) = (IE + EA) / 2 ……………….. (4)

Global softness (S) is the opposite of global hardness [17]. Softness is an additional factor to evaluate the stability and reactivity of the molecules. A High softness value results in less stability and higher inhibitory efficiency

Global softness (S) = 1/η ……………….. (5)

The global electrophilicity index (ω), which is introduced by parsing, is used to quantify stability after a molecule takes an increased number of electrons [18]. appropriate inhibitors with a lower global electrophilicity index value.

electrophilicity index (ω) = $(-\chi)^2/ 2\eta$ ……………….. (6)

However, the predicted values of 7.0 eV mol-1 and 0.0 eV mol-1 for mild steel, respectively, were also used to show the quantity of electrons transferred (ΔN) from the inhibitor to the carbon steel surface. The ΔN according to PM3 and DFT results, values are associated with inhibitory efficiency [19], which is displayed in Tables 2 and 4. According to experimental considerations, the best inhibition efficiency occurs when [A] electrons move from lower χ to higher χ until the chemical potentials equalize. For instance, electrons will go from an inhibitor to Fe if two systems, Fe and inhibitor, are combined to create (ΔN). This is also determined using the equation [20]:

Electrons transferred (ΔN) = $(\chi_{Fe} - \chi_{inhib.})/ [2 (\eta_{Fe} + \eta_{inhib.})]$ …… (7)

A high value of ΔN (especially >3) indicates strong tendency to the electrons are donate to surface of metal a higher inhibitory efficiency [21].

The absolute electronegativity of iron is represented by χ_{Fe}, whereas the electronegativity of the inhibitor molecule is represented by χ_{inhib}. The absolute hardness of the inhibitor molecule and iron is represented by η_{Fe} and η_{inhib}, respectively. Another important electronic characteristic is the dipole moment (μ in Debye), which is the result of the distance between the two bound atoms and the uniform charge distribution on the atoms. By affecting the transport process via the adsorbed layer, high dipole moment values are said to promote adsorption and, hence, the efficacy of inhibition rises with dipole moment values [22]. According to Tables 3 and 5, the dipole moments of [A] compound is (9.9757) Debye for the PM3 approach and (3.2687) Debye for the DFT method. Strong dipole-dipole interactions are likely indicated by metallic surfaces with these chemicals. Compared to other work [23] the inhibition efficiency of the inhibitor molecule [A] is higher according to DFT calculations is indicated by the limits efficiency as shown in Tables 6, and also the Quantum parameters for the inhibitor molecule [A] calculated by using the PM3 method as shown in Table 4.

Table 3. The calculated quantum chemical parameters for compound [A] by using the PM3 method.

Parameters of Inhibitor	**[A]**
Molecular formula	$C_{21}H_{18}N_4O_3S_2$
m.wt. (g/mol)	438.52
Point group	C1
E_{LUMO} (ev)	1.7309
E_{HOMO} (ev)	-3.6181
ΔE (ev)	5.3491
Dipole moment (Debye)	9.9757

Table 4. Quantum parameters for the inhibitor molecule [A] calculated by using the PM3 method.

Parameters of Inhibitor	**PM3**
IP (eV)	3.6181
EA (eV)	1.7309
η (eV)	0.9436
χ (eV)	2.6745
S (eV)	1.05977
ω (eV)	3.74843
ΔN (eV)	2.29201

Table 5. The calculated quantum chemical parameters for compound [A] by using the DFT method.

Parameters of Inhibitor	**DFT (6-311G/ B3LYP)**	
	[A]	**other work [23]**
Molecular formula	$C_{21}H_{18}N_4O_3S_2$	--------
m.wt. (g/mol)	438.52	335.15
Point group	C1	--------
ELUMO (ev)	0.2519	0.640
EHOMO (ev)	-1.9015	–5.963
ΔE (ev)	2.1534	6.603
Dipole moment (Debye)	3.2687	----------

Table 6. Quantum parameters for the [A] inhibitor molecule calculated by using the DFT method.

Parameters of Inhibitor	DFT (6-311G/ B3LYP)	other work[23]
IP (eV)	1.1486	-0.640
EA (eV)	0.3246	5.963
η (eV)	0.412	3.301
χ (eV)	0.7366	2.648
S (eV)	2.4271	0.303
ω (eV)	0.65847	1.062
ΔN (eV)	7.60121	0.367

Local reactivity of the two inhibitors

The DFT and PM3 Mulliken charges population analysis, which is a sign of reactive molecular centers (nucleophilic and electrophilic centers), is used to examine the native reactivity of the inhibitors under study. The electron density is crucial in determining the chemical reactivity since molecules with a high electronic charge are chemically softer than those with a low charge. Chemical adsorption contacts are also orbital or electrostatic interactions. The electrical charges of the molecule determined the electrostatic interactions' driving force. In physicochemical reactions, however, charges are crucial characteristics [24]; just the charges for nitrogen (N), oxygen (O), sulfur (S), and a few carbon atoms are shown.

Therefore, the place with the highest negative charge value will be the nucleophilic assault site. Conversely, the positive charge value of the most electron-accepting, reactive sites governed the electrophilic attack site, as shown in Figure (3). Therefore, C_6, S_8, S_9, C_{14}, C_{22}, C_{33} and C_{40} are the locations that [A] compound prefers to attack electrophilicity. In order to create feedback bonds and strengthen the connection between the inhibitor and the metal surface, these atoms take electrons from the 3d orbitals of the metal atoms. Therefore, the atoms with negative charges are represented by the favored nucleophilic sites in [A] compound. Reactive sites that can give metals electrons should be the target of nucleophilic assaults. The atomic charge for two inhibitors is displayed in Table 7. The two inhibitors have multiple functional sites for adsorption on metal surfaces, including (N, O, S) atoms and ring electrons, which give electrons to metal surfaces for bonding, according to the data above. However, due to its single pair of electrons and empty d orbitals, the S atom is able to give and receive electrons from the metal. Furthermore, the active sites have a [A] molecule's shape, which is planner, (Fig.1). This contributes electrons to the metal surface, which facilitates the adsorption of compound [A] [4].

Table 7. Mullikan charge distribution on atoms of compound [A] by using PM3 and DFT methods

Symbol of atom	Atomic charge		Symbol of atom	Atomic charge	
	PM3	DFT		PM3	DFT
N_1	0.178	-0.728	C_{24}	-0.077	-0.001
C_2	-0.208	-0.264	C_{25}	-0.078	-0.122
C_3	-0.144	-0.632	H_{26}	0.129	0.145
C_4	-0.586	-0.202	C_{27}	-0.155	-0.226
N_5	0.344	-0.758	H_{28}	0.110	0.135
C_6	-0.125	0.467	H_{29}	0.100	0.124
C_7	-0.243	-0.441	H_{30}	0.104	0.123
S_8	0.257	0.341	N_{31}	-0.023	-0.395
S_9	0.283	0.269	O_{32}	-0.389	-0.405

C_{10}	-0.098	-0.060	C_{33}	-0.253	0.200
C_{11}	-0.050	-0.181	C_{34}	-0.174	-0.109
C_{12}	-0.081	-0.193	C_{35}	-0.133	-0.120
C_{13}	-0.138	-0.137	C_{36}	-0.039	-0.174
C_{14}	0.239	0.522	H_{37}	0.092	0.179
H_{15}	0.054	0.195	C_{38}	-0.065	-0.161
H_{16}	0.075	0.199	H_{39}	0.101	0.164
H_{17}	0.073	0.204	C_{40}	-0.624	0.289
H_{18}	0.136	0.196	H_{41}	0.106	0.184
H_{19}	0.104	0.141	H_{42}	0.109	0.182
H_{20}	0.102	0.141	N_{43}	1.329	-0.049
H_{21}	0.096	0.129	O_{44}	-0.701	-0.360
C_{22}	0.011	0.283	O_{45}	-0.709	-0.360
C_{23}	-0.141	-0.116			

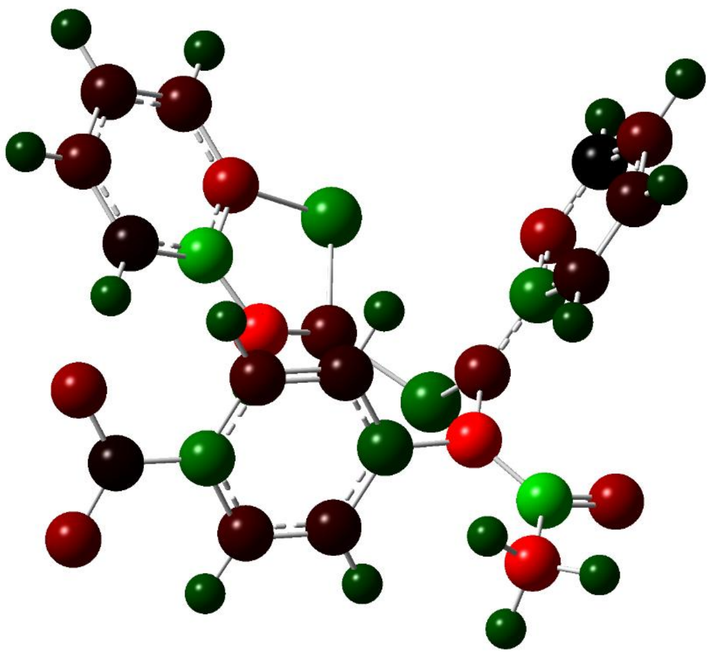

Figure 3. The charge distribution of compound [A]

4. Conclusion

In this study, quantum mechanical calculations of PM3 and DFT (B3LYP) using (6-311G) (2d,2p) were theoretically identified as stronger corrosion inhibitor. Physical characteristics and quantum chemical parameters were linked to the inhibition efficacy of two inhibitors tested in the geometry of equilibrium. According to theoretical inhibition parameters, the compound [A] is high inhibitor efficiency . The geometric structures revealed that the compound [A] reactive sites were planner, making it a more effective corrosion inhibitor. The reactive site was appropriately estimated by the DFT Mulliken charges for electrophilic and nucleophilic.

REFERENCES

[1] D. A. David, “Predicting the performance of organic corrosion inhibitors,” *Metals*, vol. 7, no. 553, pp. 1–8, 2017.

[2] Y. El-Bakri, M. Boudalia, S. Echihi, A. Harmaoui, J. Sebhaoui, H. Elmsellem, *et al.*, “Performance and theoretical study on corrosion inhibition of new triazolopyrimidine derivative for carbon steel in hydrochloric acid,” *J. Mater. Environ. Sci.*, vol. 8, no. 2, pp. 378–388, 2017.

[3] R. M. Kubba, M. A. Mohammed, and L. S. Ahamed, “DFT calculations and experimental study to inhibit carbon steel corrosion in saline solution by quinoline-2-one derivative,” *Baghdad Sci. J.*, vol. 18, no. 1, p. 16, 2021.

[4] A. H. Radhi, E. A. Du, F. A. Khazaal, Z. M. Abbas, O. H. Aljelawi, S. D. Hamadan, *et al.*, "HOMO-LUMO energies and geometrical structures effect on corrosion inhibition for organic compounds predicted by DFT and PM3 methods," *NeuroQuantology*, vol. 18, no. 1, pp. 37–45, 2020.

[5] M. Yadav, S. Kumar, D. Behera, I. Bahadur, and D. Ramjugernath, "Electrochemical and quantum chemical studies on adsorption and corrosion inhibition performance of quinoline-thiazole derivatives on mild steel in hydrochloric acid solution," *Int. J. Electrochem. Sci.*, vol. 9, pp. 5235–5257, 2014.

[6] Y. E. Louadi, F. Abrigach, A. Bouyanzer, R. Touzani, A. El Assyry, A. Zarrouk, *et al.*, "Theoretical and experimental studies on the corrosion inhibition potentials of two tetrakispyrazole derivatives for mild steel in 1.0 M HCl," *Port. Electrochim. Acta*, vol. 35, no. 3, pp. 159–178, 2017.

[7] W. Kitagawa and T. Tamura, "Quinoline, antibiotic from *Rhodococcus erythropolis* JCM 6824," *J. Antibiot.*, vol. 61, no. 11, pp. 680–682, 2008.

[8] R. M. Kubba, D. A. Challoob, and S. M. Hussen, "Quantum mechanical and electrochemical study of new isatin derivative as corrosion inhibitor for carbon steel in 3.5 % NaCl," *Int. J. Sci. Res.*, vol. 6, no. 7, pp. 1656–1669, 2017.

[9] S. B. Ade, "Corrosion inhibition analysis of mild steel in various acid medium by amide (-$CONH_2$) group of organic compounds," *World J. Pharm. Res.*, vol. 11, pp. 1525–1535, 2022.

[10] R. M. Kubba and M. M. Khathem, "Theoretical studies of corrosion inhibition efficiency of two new N-phenyl-ethylidene-5-bromo isatin derivatives," *Iraqi J. Sci.*, pp. 1041–1051, 2016.

[11] V. Sathyanarayanmoorthi, R. Karunathan, and V. Kannappan, "Molecular modeling and spectroscopic studies of benzothiazole," *J. Chem.*, vol. 2013, pp. 1–8, 2013.

[12] G. Gece, "The use of quantum chemical methods in corrosion inhibitor studies," *Corros. Sci.*, vol. 50, pp. 2981–2992, 2008.

[13] N. A. Lafta, "Theoretical spectroscopic study for some thiophene derivatives," M.Sc. thesis, Al-Nahrain University, Baghdad, Iraq, 2017.

[14] B. Lin and Y. Zuo, "Corrosion inhibition of carboxylate inhibitors with different alkylene chain lengths on carbon steel in an alkaline solution," *RSC Adv.*, vol. 9, pp. 7065–7077, 2019.

[15] L. Guo, Z. S. Safi, S. Kaya, W. Shi, B. Tüzün, N. Altunay, and C. Kaya, "Anticorrosive effects of some thiophene derivatives against the corrosion of iron: A computational study," *Front. Chem.*, vol. 6, p. 155, 2018.

[16] I. Ahamad, R. Prasad, and M. A. Quraishi, "Thermodynamic, electrochemical and quantum chemical investigation of some Schiff bases as corrosion inhibitors for mild steel in hydrochloric acid solutions," *Corros. Sci.*, vol. 52, no. 3, pp. 933–942, 2010.

[17] R. P. Sonawane and R. R. Tripathi, "The chemistry and synthesis of 1H-indole-2,3-dione (isatin) and its derivatives," *Int. Lett. Chem., Phys. Astron.*, vol. 7, no. 1, pp. 30–36, 2013.

[18] F. Bentiss, M. Lebrini, and M. Lagrenée, "Thermodynamic characterization of metal dissolution and inhibitor adsorption processes in mild steel/2,5-bis(n-thienyl)-1,3,4-thiadiazoles/hydrochloric acid system," *Corros. Sci.*, vol. 47, no. 12, pp. 2915–2931, 2005.

[19] N. Khalil, "Quantum chemical approach of corrosion inhibition," *Electrochim. Acta*, vol. 48, no. 18, pp. 2635–2640, 2003.

[20] P. Zhao, Q. Liang, and Y. Li, "Electrochemical, SEM/EDS and quantum chemical study of phthalocyanines as corrosion inhibitors for mild steel in 1 mol/l HCl," *Appl. Surf. Sci.*, vol. 252, no. 5, pp. 1596–1607, 2005.

[21] E. Lukovits, E. Kálmán, and F. Zucchi, "Corrosion inhibitors—Correlation between electronic structure and efficiency," *Corrosion*, vol. 57, pp. 3–8, 2001

[22] I. B. Obot and N. O. Obi-Egbedi, "Theoretical study of benzimidazole and its derivatives and their potential activity as corrosion inhibitors," *Corros. Sci.*, vol. 52, no. 2, pp. 657–660, 2010.

[23] K. Azgaou, R. Hsissou, K. Chkirate, M. Benmessaoud, M. Hefnawy, A. El Gamal, *et al.*, "Corrosion inhibition and adsorption properties of N-{2-[2-(5-methyl-1H-pyrazol-3-yl)acetamido] phenyl} benzamide monohydrate on C38 steel in 1 M HCl: Insights from electrochemical analysis, DFT, and MD simulations," *ACS Omega*, vol. 10, no. 6, pp. 6244–6257, 2025.

[24] H. Wang, X. Wang, H. Wang, L. Wang, and A. Liu, "DFT study of new bipyrazole derivatives and their potential activity as corrosion inhibitors," *J. Mol. Model.*, vol. 13, no. 1, pp. 147–153, 2007.